Interseismic Velocity Field and Seismic Moment Release in Northern Baja California, Mexico

by J. Alejandro González-Ortega, J. Javier González-García, and David T. Sandwell

ABSTRACT

We have analyzed all available continuous Global Positioning System (cGPS) and campaign-mode GPS data from northern Baja California, Mexico, covering the 1993.1–2010.1 period to obtain a consistent interseismic velocity field to derive a continuous strain-rate field. The analysis shows concentrations of high strain rate along the Imperial/Cerro Prieto fault system extending from the Salton Sea to the Gulf of California, with strike-slip faulting consistent with principal strain axes direction within the area of largest historical and instrumental seismic release. We translated the strain rate into geodetic moment accumulation rate to evaluate the potential of seismic activity of the region and compare with the actual seismic release of historical and instrumental earthquake catalog. Comparison of regional moment accumulation rate based on geodesy ($\dot{M}_0^g = 6.3 \pm 1.3 \times 10^{18}$ N · m/yr) to the corresponding moment release rate by earthquakes ($\dot{M}_0^s = 2.7 \pm 0.8 \times 10^{18}$ N · m/yr) highlights a moment rate deficit equivalent to an M_w 7.5–7.8 earthquake. As part of this accumulated moment was released by the recent 2010 M_w 7.2 El Mayor–Cucapah earthquake, these results can provide input constraints on earthquake forecasts for the northern Baja California fault system.

Electronic Supplement: Tables of Global Positioning System (GPS) velocities, earthquake catalog, and figures comparing interpolation methods and earthquake catalogs.

INTRODUCTION

The seismicity and tectonics of northern Baja California is dominated by right-lateral slip (48–52 mm/yr) along the San Andreas fault system, which forms the boundary between Pacific and North American plates (Argus *et al.*, 2010; DeMets *et al.*, 2010) (Fig. 1, inset). The major faults of the region include the southern Elsinore and San Jacinto faults, Imperial, Cerro Prieto, Pescaderos-Indiviso, Laguna Salada, San Miguel-Vallecitos, and Agua Blanca faults (Darby *et al.*, 1984; Frez and Gonzalez, 1991; Gonzalez-Garcia *et al.*, 2010). At the latitude of California and Baja California international border, ~80% of the slip occurs on the Imperial, Cerro Prieto, and nearby faults (Bennett *et al.*, 1996). As a result, the Imperial and Mexicali Valleys have the most active level of seismicity in southern California and northern Baja California.

Seismic potential can be estimated as the difference between the geodetically measured moment accumulation and the seismic moment released by earthquakes (e.g., Ward, 1998; Pancha *et al.*, 2006). Detailed maps of the crustal velocity field can be used to construct maps of moment accumulation rate; likewise, seismicity maps can be used to construct maps of moment release rate. Comparison of these maps reveals regions of high- and low-seismic potential (e.g., Bos and Spakman, 2005; Masson *et al.*, 2005; Meade and Hager, 2005; Mazzotti *et al.*, 2011; D'Agostino, 2014) and thus bounds on earthquake rupture forecast models (Field *et al.*, 2014).

Here, we develop a horizontal crustal velocity model for the southernmost San Andreas system using all continuous Global Positioning System (cGPS) and campaign-mode GPS for the interseismic time period 1993.1–2010.1. From this model, we construct maps of strain rate and strain orientation as well as maps of moment accumulation rate assuming a uniform-thickness seismogenic layer. Based on the major faults of the region, the maps are divided into zones and the moment accumulation in each zone is compared with historical seismicity to assess seismic potential of the major faults.

GPS NETWORK, CRUSTAL VELOCITY, STRAIN FIELD, AND GEODETIC MOMENT

GPS studies in northern Baja California started in early 1990s by a number of collaborating institutions, including the Salton Trough Riverside County group, University of Miami, and Centro de Investigación Científica y de Educación Superior de Ensenada (CICESE). These survey-mode geodetic monuments (Fig. 1) consist of stainless steel screws cemented into

 doi: 10.1785/0220170133

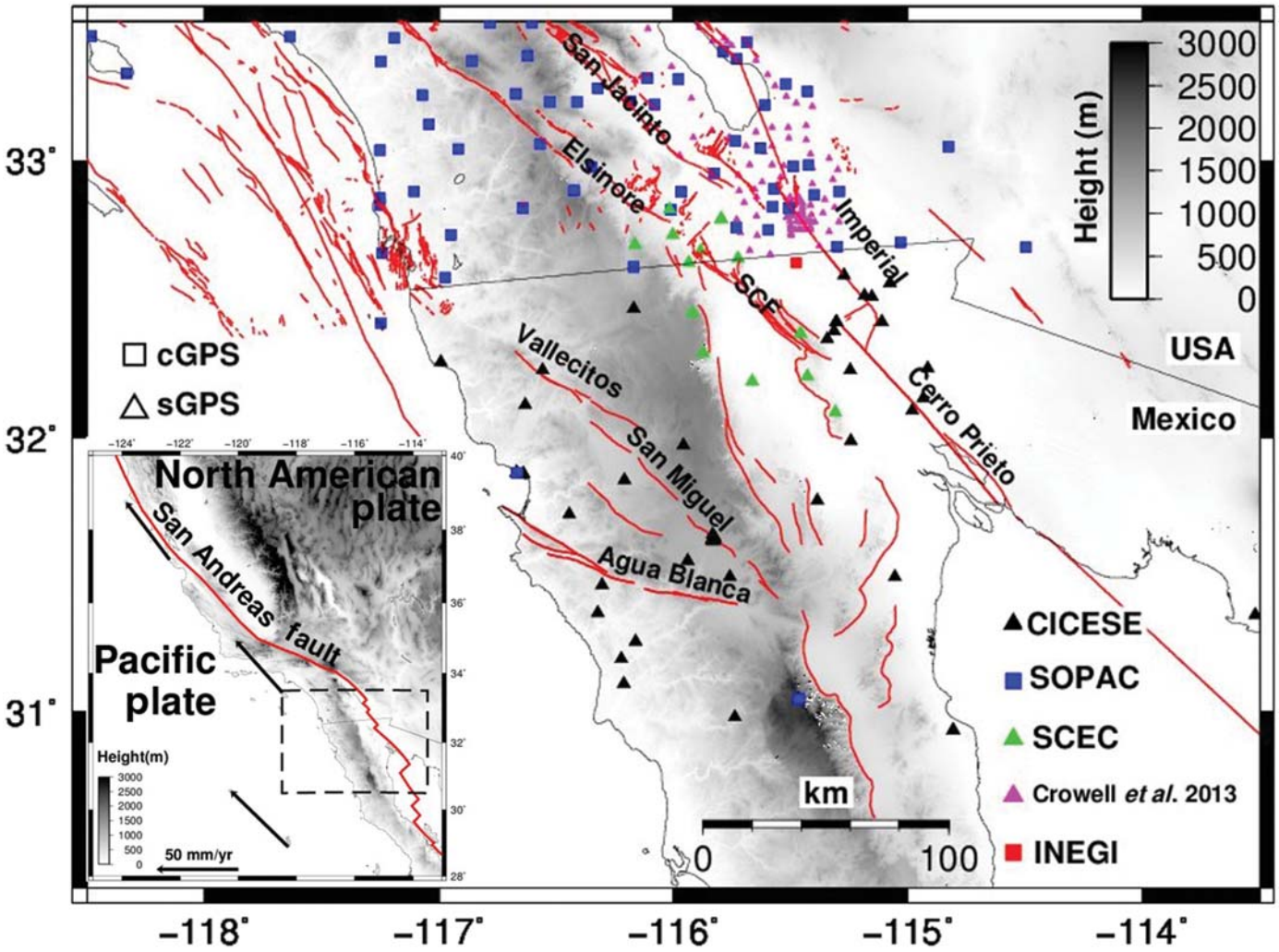

▲ **Figure 1.** Global Positioning System (GPS) Network in southern California and northern Baja California. Blue squares correspond to continuous GPS network by Scripps Orbit and Permanent Array Center (SOPAC) (60 sites); black, green, and magenta color squares are survey monument occupations (177 sites). Red lines denote known active faults from U.S. Geological Survey fault database and from Darby *et al.* (1984). INEGI, Instituto Nacional de Estadística y Geografía (Mexico). (Inset) Broader tectonic setting of the study area. Black vectors show the tectonic motion with respect to North American plate.

host rock structures for long-term semiperiodic temporal survey GPS (sGPS) occupations and have been used to study crustal deformation, including horizontal site velocity to constrain slip rates on major faults according to different rheology models, constrains estimates for Pacific and North America plates motion, and to test the coupled nature of the Baja California microplate (Bennett *et al.*, 1996; Dixon *et al.*, 2002; Gonzalez-Garcia *et al.*, 2003; Platnner *et al.*, 2007; Shen *et al.*, 2011). Data from 1993 to 2002 are archived at the Southern California Earthquake Center (SCEC) and UNAVCO database servers, whereas the most recent data from 2002 to 2010 are stored at CICESE. Recently installed cGPS sites since the occurrence of the El Mayor–Cucapah earthquake (e.g., Hauksson *et al.*, 2010; Huang *et al.*, 2016) have been used to study postseismic transient deformation using different rheological models that best explain the data (Pollitz *et al.*, 2012; Gonzalez-Ortega *et al.*, 2014; Spinler *et al.*, 2015).

We estimated the interseismic crustal velocity sites for northern Baja California, covering the 1993.1–2010.1 period, by processing the GPS data with the GAMIT/GLOBK processing package, v.10.6 (Herring *et al.*, 2015). As we have different GPS data sources (Antonelis *et al.*, 1999; Dixon, 2000, 2004), we did a full review of receiver, antenna type, and height of instrument, as a function of time occupation of GPS stations. GAMIT software uses double-difference phase data between GPS satellites and stations to solve for station coordinates, atmospheric zenith delays, and integer ambiguities for a full UTC day in a loosely constrained solution covariance matrix. Next, GLOBK software is used to estimate velocities by combining the loosely constrained solution with the International Global Navigation Satellite Service (IGS) solution from Scripps Orbit and Permanent Array Center (SOPAC) for all surveyed sites in the ITRF2008 reference frame. The site velocities are estimated by least-squares linear

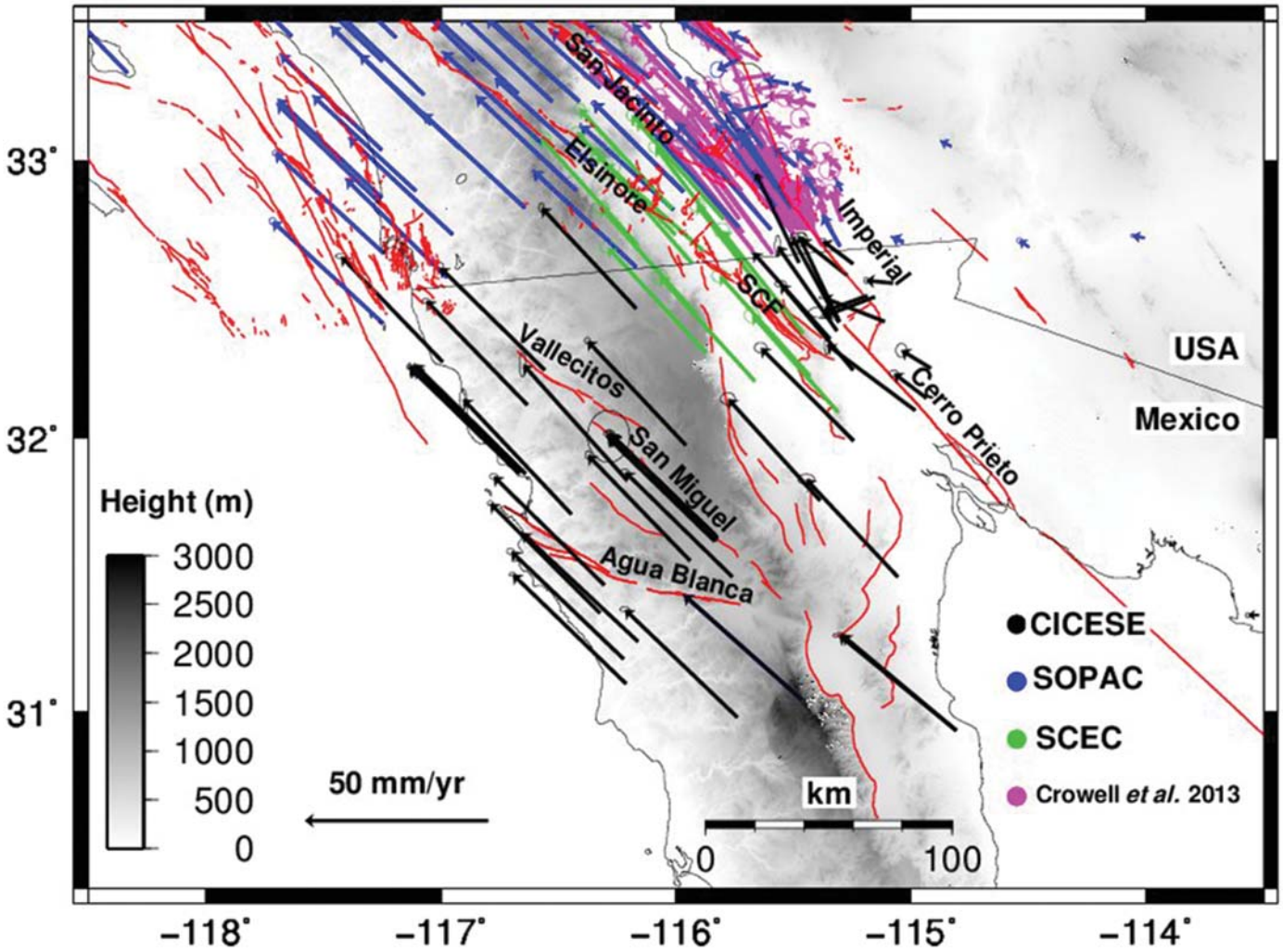

▲ **Figure 2.** Crustal velocity field of velocity data in northern Baja California derived from 1993.1 to 2010.1 GPS observations in Stable North America Reference Frame. Blue arrows, velocity provided by SOPAC; magenta arrows, velocity from Crowell *et al.* (2013); green arrows, velocity from Southern California Earthquake Center (SCEC) Crustal Motion Map version 4. Black vectors are GPS velocities from this study.

fitting to time variation of coordinates for each station (e.g., Herring, 2003; see Ⓔ Tables S1–S3, available in the electronic supplement to this article).

Crustal velocity sites obtained here (crustal velocity northern Baja California [CVNB]) are complemented by three additional sources of information: the SOPAC (see Data and Resources) database which contains cGPS measurements in southern California since 1990 to date, the Salton trough high-resolution interseismic velocity (STIV) (Crowell *et al.*, 2013), and the SCEC Crustal Motion Map version 4 (CMM4) (Shen *et al.*, 2011). In particular, velocity sites results for 13 geodetic observations (1978–1991) with electronic distance measurement (EDM) technique in the mountains surrounding the depression of Laguna Salada (Savage *et al.*, 1994) is presented with respect to Stable North America Reference Frame (SNARF; Blewitt *et al.*, 2005). To merge the different databases (60 cGPS and 164 sGPS sites) to a common reference frame, the SOPAC, STIV, and CVNB were rotated into SNARF (Fig. 2). In general, sites distribution is concentrated in northern part of Imperial fault in U.S. side of the border and fairly homogeneous over the peninsular ranges in southern California and northern Baja California. GPS observations inside Cerro Prieto Geothermal Field were removed from the subsequent strain-rate analysis because they have large signals caused by fluid extraction (e.g., Glowacka *et al.*, 2009; Sarychikhina *et al.*, 2011; see Ⓔ Table S2).

Various methods can be used to derive regional strain-rate field from GPS velocity data, ranging from Delaunay triangulation with computation of internal strain rate to spline functions in self-consistent interpolated velocity gradient tensor field (e.g., Haines and Holt, 1993; Kreemer *et al.*, 2014). Here, we used two interpolation methods to construct surface interpolated velocity field: using Green's functions in an elastic deformation media (Sandwell and Wessel, 2016) and spline interpolation of GPS velocity components (Wessel and Bercovici, 1998; Hackl *et al.*, 2009). Both methods show similar

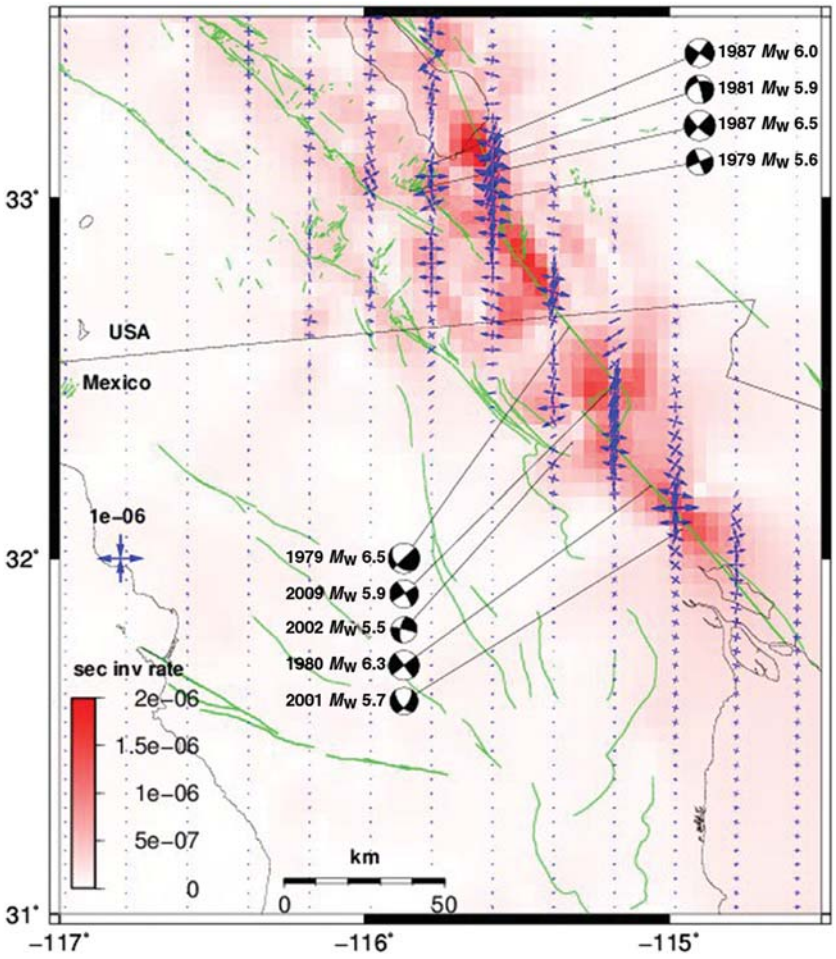

▲ **Figure 3.** Map of second invariant strain-rate magnitude (see color bar) and principal horizontal axes obtained from interpolated velocity field. Earthquake focal mechanisms for $M_w \geq 5.5$ from 1979 to 2009 (Dziewonski *et al.*, 1981; Ekström *et al.*, 2012).

results (see Ⓔ Fig. S1 and GPS data interpolation). However, subsequent strain-rate field is carried out using the Sandwell and Wessel (2016) method, as it uses elasticity theory to couple the east and north velocity components (Haines and Holt, 1993), which provides better results in areas where the distribution of observed velocities is dense.

A 2D strain-rate tensor field can be constructed from the vector velocity field

$$\dot{\varepsilon}_{1,2} = \frac{\dot{\varepsilon}_{ee} + \dot{\varepsilon}_{nn}}{2} \pm \sqrt{\left\{\frac{1}{4}(\dot{\varepsilon}_{ee} - \dot{\varepsilon}_{nn})^2 + \dot{\varepsilon}_{en}^2\right\}} \quad (1)$$

$$\tan 2\theta = \frac{2\dot{\varepsilon}_{en}}{\dot{\varepsilon}_{en} - \dot{\varepsilon}_{nn}} \quad (2)$$

$$\dot{\varepsilon} = \sqrt{\dot{\varepsilon}_{ee}^2 + \dot{\varepsilon}_{nn}^2 + 2\dot{\varepsilon}_{en}^2}, \quad (3)$$

(Turcotte and Shubert, 2002), with $\dot{\varepsilon}_{ee} = \frac{\partial v_e}{\partial x_e}$, $\dot{\varepsilon}_{nn} = \frac{\partial v_n}{\partial x_n}$, $\dot{\varepsilon}_{en} = \frac{1}{2}\left(\frac{\partial v_e}{\partial x_n} + \frac{\partial v_n}{\partial x_e}\right)$, in which v_n and v_e are the north and east velocity field components, respectively. The first and second terms of the right side of equation (1) represent the dilatant strain rate and the maximum shear-strain rate, respectively; equation (2) provides the direction θ of the main deformation axes, and equation (3) is the second invariant of the strain rate. Interpolated velocity field with elementary cell of 5 km by 5 km, is used to calculate the strain components with the same grid spacing.

The principal axes and second invariant strain rate (Fig. 3) roughly follow the location of the Imperial and Cerro Prieto faults (e.g., Wdowinski *et al.*, 2001). There, ~25-km-wide continuous deforming belt is characterized by ~1.5 μstrain/yr. Part of these high shear-strain rates is attributable to aseismic creep in the northern segment of the Imperial fault (Lyons *et al.*, 2002; Crowell *et al.*, 2013). In contrast, no horizontal aseismic creep has yet been observable in Cerro Prieto fault trace (e.g., Samsonov *et al.*, 2017; Xu *et al.*, 2017). High strain rates in aseismic zones do not necessarily correspond to high-seismic hazard, because part of the deformation is not accumulated as elastic energy (e.g., Field *et al.*, 2014). Focal mechanisms for recent earthquakes (Dziewonski *et al.*, 1981; Ekström *et al.*, 2012) are consistent with the deformation field, compatible with a northwest right-lateral motion between the Pacific and North American plates, and with strike-slip and dip-slip faulting along the Imperial/Cerro Prieto fault system (Frez and Gonzalez, 1991). For instance, principal tension and compressional axes orientations from recently reviewed $M_w > 6.0$ earthquakes (Southern California Earthquake Center [SCEDC], 2013) show good agreement when compared with principal strain axes (Fig. 3).

Principal strain rates are used to estimate the geodetic moment accumulation rate (Savage and Simpson, 1997; Ward, 1998), with

$$\dot{M}_0^g = 2\mu AH \max(|\dot{\varepsilon}_1|, |\dot{\varepsilon}_2|, |\dot{\varepsilon}_1 + \dot{\varepsilon}_2|), \quad (4)$$

in which, μ is the shear modulus (3×10^{10} N/m^2), A is the size of the elementary cell resolution (5 km by 5 km), H is the seismogenic thickness, and max function extracts the largest value of the principal strain rate. The major assumptions in this analysis are (1) all of the strain will be relieved elastically so there is no plastic deformation in the plate and (2) the effective thickness of the locked zone on each fault is equal to the assumed seismogenic thickness. Modeling of dense GPS surveys (Lyons *et al.*, 2002) as well as Interferometric Synthetic Aperture Radar data (Lindsey and Fialko, 2016) across the Imperial fault show it has significant shallow and sometimes episodic creep resulting in an effective locking thickness of only

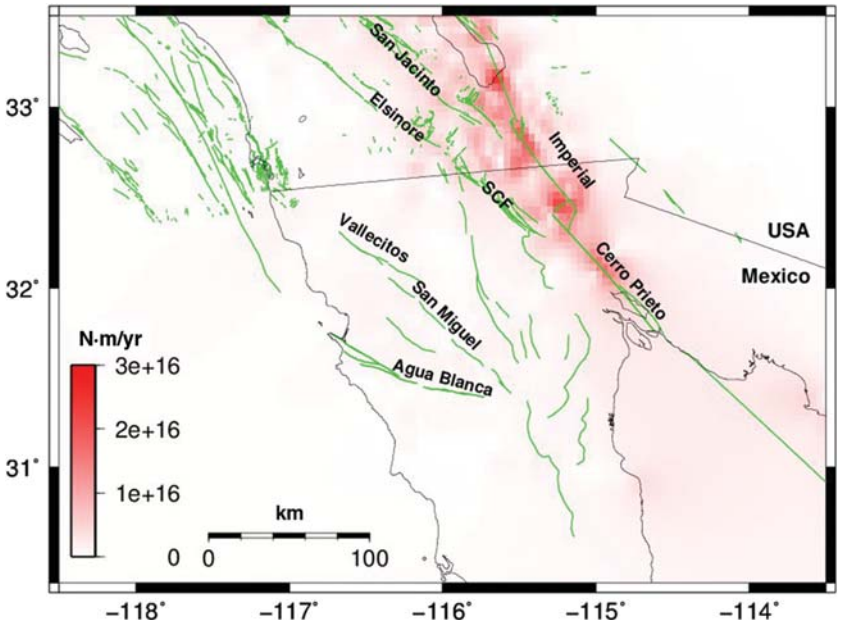

▲ **Figure 4.** Map of geodetic moment accumulation rate considering seismogenic thickness of $H = 10$ km.

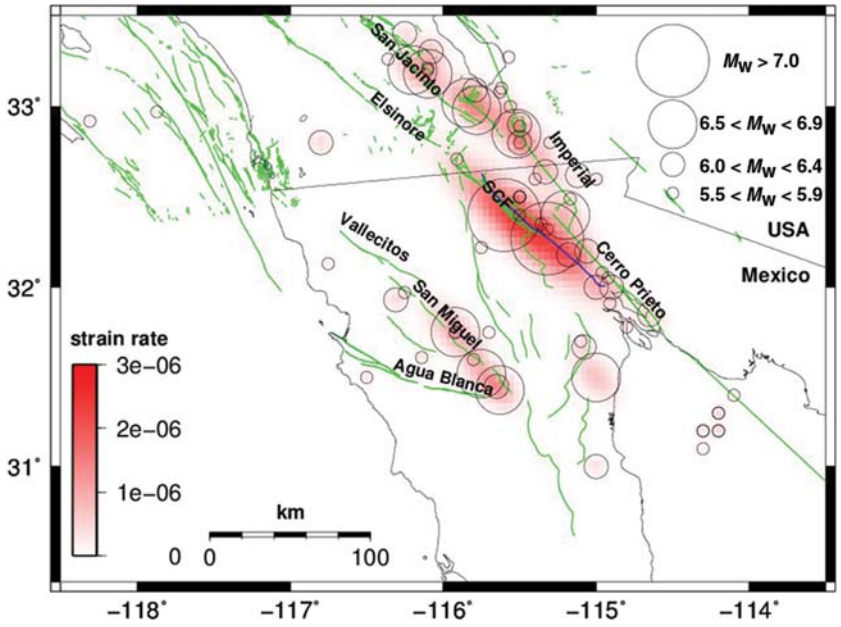

▲ **Figure 5.** Seismicity distribution of historic and instrumental earthquake catalog for $M_w \geq 5.5$ since 1891–2017. Superimposed is the calculated seismic strain rate. The blue line denotes the El Mayor–Cucapah 2010 earthquake fault trace.

7 km. Nevertheless, we use a constant seismogenic thickness of $H = 10$ km for the inland region (Frez and Gonzalez, 1991) enclosed by San Jacinto, Elsinore, Sierra Cucapah, Imperial, Cerro Prieto, San Miguel, Vallecitos, and Agua Blanca faults. Because of incomplete fault locking as well as plastic deformation, we obtain and upper bound on the geodetic moment accumulation rate of $\dot{M}_0^g = 6.3 \pm 1.3 \times 10^{18}$ N · m/yr (Fig. 4).

SEISMIC MOMENT RELEASE AND STRAIN FIELD

The historical catalog of earthquakes in northern Baja California dates back to November 1852, when an earthquake M_w 6–7 occurred, possibly associated with the Cerro Prieto fault, whose main feature was the appearance of a geyser high enough to have been observed from Fort Yuma, Arizona (Wallace, 1990). Here, we used the compilation of historical and instrumental seismic catalog for $M_w \geq 5.5$ in the time interval 1891.6–2017.0 (Felzer and Cao, 2008; Hutton *et al.*, 2010) (Ⓔ Table S4 and Figs. S2 and S3). Compilation of earthquake catalog was based on three considerations: time, magnitude, and earthquake localization. For magnitude and time period from 1891 to 1932, we used Felzer and Cao (2008), except for 1892 M_w 7.1–7.3 Laguna Salada earthquake (Rockwell *et al.*, 2015). From 1932 to 2017, we used Hutton *et al.* (2010) and the seismic database from Red Sismica del Noroeste de Mexico (see Data and Resources). Some moderate earthquakes in northern Baja California such as 1956 San Miguel, 1976 Mesa de Andrade, and 1915 and 1980 Cerro Prieto (Frez and Gonzalez, 1991, and references herein) were located according to their fault ruptured traces.

Seismic strain constrains the plate deformation properties because it gives the amount of strain released by the sequence of earthquakes. The estimate of seismic strain is based on the scalar moment M_0 of the earthquakes as related to the seismic part of the strain (Kostrov, 1974; Sabadini, 2009). Figure 5 shows the geographical distribution of earthquakes, with $M_w \geq 5.5$ superimposed on the seismic strain rates, obtained from a modified Kostrov equation, where each earthquake has a bilateral rupturing pattern which involves strain-rate effect that is spatially distributed as elliptical Gaussian function (methodology for deriving seismic strain rates is available in the Ⓔ electronic supplement), according to

$$\dot{\varepsilon} = \frac{1}{2\sqrt{2\pi}\mu HT} \sum_{n=1}^{N} \frac{1}{\sigma_{x_n}\sigma_{y_n}} M_n \exp(-r_n), \qquad (5)$$

in which, $\dot{\varepsilon}$ is the strain rate, μ is the shear modulus (3×10^{10} N/m^2), H is the seismogenic thickness, M_n is the seismic moment of the nth earthquake from the N total earthquakes occurring during the time interval T, and r_n is the distance of the nth earthquake. σ_{xn} is associated with the length of the rupture and σ_{yn} is the perpendicular length to the rupture. σ_{xn} and σ_{yn} represent an area of influence around the nth earthquake where the elastic effects of the rupture are significant (see Ⓔ Figs. S4 and S5).

The 75 $M_w \geq 5.5$ earthquakes from 1891.6 to 2017.0 in the border region between northern Baja California and southern California gives a seismic moment of $\dot{M}_0^s = 3.4 \pm 1.0 \times 10^{20}$ N · m (moment release rate of $\dot{M}_0^g = 2.7 \pm 0.8 \times 10^{18}$ N · m/yr). To take into account the seismic moment released by $M_w < 5.5$ earthquakes (e.g., Chousianitis *et al.*, 2015), we applied the methodology proposed by Molnar (1979). This estimate is less than 10% of the total seismic moment obtained here. Seismic events in Imperial, Cerro Prieto, and Sierra Cucapah faults contribute to 68% of seismic moment release, $\dot{M}_0^s = 2.3 \times 10^{20}$ N · m, including the 1892 Laguna Salada M_w 7.2, 1915 and 1934 Colorado River Delta M_w 6.6 and 6.4, 1940 Imperial Valley M_w 6.9, and 2010 El Mayor–Cucapah M_w 7.2 earthquakes (Fig. 5). Most of the rest seismic moment release in the Baja California and California border region is caused by the 1903 M_w 6.6 earthquake that occurred in the vicinity of Sierra Las Pintas/Sierra San Pedro Mártir, the 1954 and 1956 M_w 6.8–6.0 earthquake swarm in San Miguel fault, and finally a series of $M_w \sim 6.5$ earthquakes associated with the southern part of San Jacinto fault.

DISCUSSION

Prominent geodetic strain is primarily distributed over Imperial and Cerro Prieto faults. For the western part of this region, the uniformity of the velocity field yields a geodetic strain less than 0.1 μstrain/yr. Seismic strain is mainly concentrated along the surface faults associated with earthquakes $M_w \geq 6.5$, and these earthquakes represent 80% of the seismic moment of northern Baja California and southern California region.

We estimated the geodetic strain rate from surface interpolated velocity field. The geodetic strain rate, in the absence of significant earthquakes or aseismic creep, is generally interpreted as the interseismic elastic loading on faults in the upper seismogenic crust, which in turn may potentially release seismicity (e.g., D'Agostino, 2014). Thus, the geodetic moment accumulation rate is compared with the seismic moment release rate evaluated by summing the contribution of earthquakes contained within the same area (fault zones). With the geodetic moment and seismic moment difference, we get the accumulated moment, and the part of it may be released as subsequent earthquakes (e.g., Ward, 1998; Meade and Hager, 2005). Moment accumulation enclosed by San Jacinto, Elsinore, Sierra Cucapah, Imperial, Cerro Prieto, San Miguel, Vallecitos, and Agua Blanca faults before El Mayor–Cucapah earthquake is equivalent to an earthquake of M_w 7.5–7.8 considering the associated uncertainties in the evaluation of geodetic and seismic moment rates (Fig. 6). With the occurrence in 2010 M_w 7.2 El Mayor–Cucapah in the southern tip of Cucapah Mountains, the overall region accumulated moment rate is reduced by ~15%. In San Miguel, Vallecitos, and Agua Blanca faults, geodetic and seismic moment release are comparable in magnitude ($\dot{M}_0^g = 4.6 \pm 0.9 \times 10^{17}$ N · m/yr, $\dot{M}_0^g = 3.6 \pm 1.1 \times 10^{17}$ N · m/yr). For San Miguel fault, the very low geodetic strain rate reflects the low-velocity field gradient, which results in long recurrence interval (e.g., Dixon *et al.*, 2002); however, the right-lateral shear

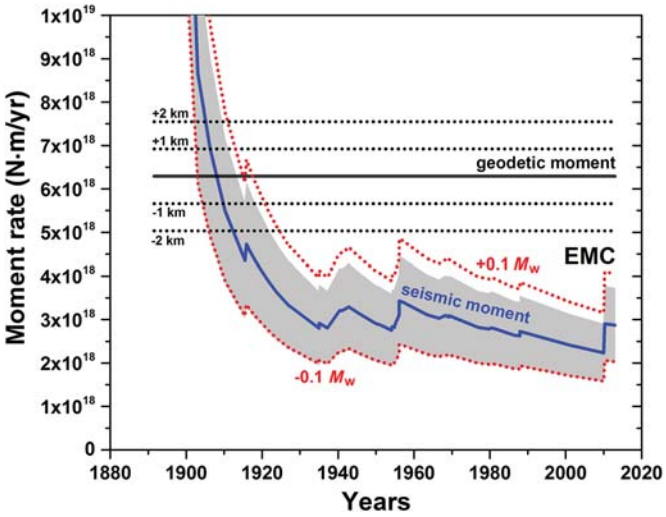

▲ **Figure 6.** Rate of seismic moment release calculated in progressively increasing time windows. The blue line corresponds to earthquake data catalog with 30% of M_0 uncertainty in gray area. Red dashed lines include total ± 0.1 M_w bias in earthquake catalog. The black line is the geodetic moment estimation, and the black dashed lines are the uncertainty considering a seismogenic depth $H = 10 \pm 1$ and $H = 10 \pm 2$ km. EMC, El Mayor–Cucapah M_w 7.2 earthquake.

rate of 0.9 ± 0.5 μstrain/yr measured using EDM technique (Darby *et al.*, 1984) indicates high localized strain rate. For Agua Blanca fault, low-velocity field gradient as well as lower seismicity (Frez *et al.*, 2000) are consistent with a locked fault and long-recurrence earthquake interval.

The moment accumulation obtained here can provide a starting point for future earthquake scenarios in the area. Given incomplete locking on the Imperial fault, the possibility of plastic deformation in the region, and lateral variations in the thickness of the seismogenic zone, this moment accumulations rate may represent an upper bound. Enhancement of recently developed Global Navigation Satellite System (GNSS) continuous network in northern Baja California, Red Geodesica del Noroeste de Mexico (see Data and Resources), and GPS temporal survey measurements across individual active faults will allow refined block models to estimate slip rates on these fault segments, as well as models based on elastic dislocation, where the geometry of the fault system is considered and its variation in the depth of the seismogenic layer (e.g., Smith-Konter *et al.*, 2011; Field *et al.*, 2014) will provide better hazard assessment estimates in northern Baja California.

CONCLUSIONS

We obtained geodetic velocities results from different GPS networks in southern California and northern Baja California. Velocity field and derived strain rates are consistent with seismic distribution of active deformation. For instance, these results confirm the general feature of Imperial/Cerro Prieto fault system such as the dominant extensional character and

its limited 50 km width of the tectonic deformation regime. Although our results should be taken with caution due to the short time period of earthquake catalog and regional extent, accumulated moment is equivalent to an earthquake of M_w 7.5–7.8, which highlights a significant deficit in seismic release in the region unless significant fraction of the geodetic moment is released aseismically, particularly in the northern part of the study area. This calls for continuing efforts to integrate GPS/GNSS networks in active deforming regions as in northern Baja California, Mexico.

DATA AND RESOURCES

Southern California Earthquake Center (SCEC) Crustal Motion Map version 4 (CMM4) can be found at http://scec.ess.ucla.edu/~zshen/cmm4/cmm4.html (last accessed April 2017). Red Sismica del Noroeste de Mexico (RESNOM) seismic database can be found at http://resnom.cicese.mx/sitio (last accessed April 2017). U.S. Geological Survey (USGS) and California Geological Survey (2017). Quaternary fault and fold database for the United States, from USGS website, available at http://earthquake.usgs.gov/hazards/qfaults/ (last accessed April 2017). Most of the figures were generated by Generic Mapping Tool (GMT) software (Wessel *et al.*, 2013). The Scripps Orbit and Permanent Array Center (SOPAC) database can be found at sopac.ucsd.edu (last accessed April 2017) and Red Geodesica del Noroeste de Mexico database can be found at http://regnom.cicese.mx (last accessed April 2017).

ACKNOWLEDGMENTS

The authors would like to thank the four anonymous reviewers and guest editor Sergio Barrientos for their valuable suggestions. This work was partially financially supported by UC-MEXUS Posdoctoral Research Project (2014–2015), Centro de Investigación Científica y de Educación Superior de Ensenada (CICESE), and the Southern California Earthquake Center (SCEC). The authors thank the support from local people during the Global Positioning System (GPS) campaigns in northern Baja California.

REFERENCES

Antonelis, K., D. J. Johnson, M. Miller, and R. Palmer (1999). GPS determination of current Pacific-North American plate motion, *Geology* **27,** 299–302.

Argus, D. F., R. G. Gordon, M. B. Heflin, C. Ma, R. J. Eanes, P. Willis, W. R. Peltier, and S. E. Owen (2010). The angular velocities of the plates and the velocity of Earth's centre from space geodesy, *Geophys. J. Int.* **180,** no. 3, 913–960.

Bennett, R. A., W. Rodi, and R. Reilinger (1996). Global Positioning System constraints on fault slip rates in southern California and northern Baja, Mexico, *J. Geophys. Res.* **101,** no. B10, 21,943–21,960.

Blewitt, G., D. Argus, R. Bennett, Y. Bock, E. Calais, M. Craymer, J. Davis, T. Dixon, J. Freymueller, T. Herring, *et al.* (2005). *A Stable North American Reference Frame (SNARF): First Release*, The SNARF Working Group, UNAVCO, Boulder, Colorado, available at https://www.unavco.org/projects/past-projects/snarf/SNARF1.0/SNARF1.0.html (last accessed April 2017).

Bos, A. G., and W. Spakman (2005). Kinematics of the southwestern U.S. deformation zone inferred from GPS motion data, *J. Geophys. Res.* **110,** no. B8, doi: 10.1029/2003JB002742.

Chousianitis, K., A. Ganas, and C. P. Evangelidis (2015). Strain and rotation rate patterns of mainland Greece from continuous GPS data and comparison between seismic and geodetic moment release, *J. Geophys. Res.* **120,** 3909–3931.

Crowell, B. W., Y. Bock, D. T. Sandwell, and Y. Fialko (2013). Geodetic investigation into the deformation of the Salton trough, *J. Geophys. Res.* **118,** no. 9, 5030–5039.

D'Agostino, N. (2014). Complete seismic release of tectonic strain and earthquake recurrence in the Appennines (Italy), *Geophys. Res. Lett.* **41,** no. 4, 1115–1162.

Darby, D., J. J. Gonzalez, and P. Lesage (1984). Geodetic studies in Baja California, Mexico, and the evaluation of short-range data from 1974 to 1982, *J. Geophys. Res.* **89,** no. B4, 2478–2490.

DeMets, C., R. G. Gordon, and D. F. Argus (2010). Geologically current plate motions, *Geophys. J. Int.* **181,** no. 1, 1–80.

Dixon, T. (2000). *Baja North 1998, UNAVCO, GPS Data Set*, available at http://www.unavco.org (last accessed April 2016).

Dixon, T. (2004). *Baja North 2001, UNAVCO, GPS Data Set*, http://www.unavco.org (last accessed April 2016).

Dixon, T., J. Decaix, F. Farina, K. Furlong, R. Malservisi, R. Bennett, F. Suarez-Vidal, J. Fletcher, and J. Lee (2002). Seismic cycle and rheological effects on estimation of present-day slip rates for the Agua Blanca and San Miguel-Vallecitos faults, northern Baja California, Mexico, *J. Geophys. Res.* **107,** no. B10, 2226–2248.

Dziewonski, A. M., T. A. Chou, and J. H. Woodhouse (1981). Determination of earthquake source parameters from waveform data for studies of global and regional seismicity, *J. Geophys. Res.* **86,** 2825–2852.

Ekström, G., M. Nettles, and A. M. Dziewonski (2012). The global CMT project 2004–2010: Centroid-moment tensors for 13,017 earthquakes, *Phys. Earth Planet. In.* **200/201,** 1–9.

Felzer, K. R., and T. Cao (2008). WGCEP historical California earthquake catalog, Appendix H in the Uniform California Earthquake Rupture Forecast, version 2 (UCERF 2), *U.S. Geol. Surv. Open-File Rept. 2007-1437H and Calif. Geol. Surv. Spec. Rept. 203H*, 127 pp.

Field, E. H., R. J. Arrowsmith, G. P. Biasi, P. Bird, T. E. Dawson, K. R. Felzer, D. D. Jackson, K. M. Johnson, T. H. Jordan, C. Madden, *et al.* (2014). Uniform California Earthquake Rupture Forecast, Version 3 (UCERF3)—The time-independent model, *Bull. Seismol. Soc. Am.* **104,** no. 3, 1122–1180.

Frez, J., and J. J. Gonzalez (1991). Crustal structure and seismotectonics of northern Baja California, in *The Gulf and Peninsular Province of the Californias*, J. P. Dauphin and B. R. Simoneit (Editors), AAPG Memoir, Vol. 47, Tulsa, Oklahoma, 261–283.

Frez, J., J. J. González, J. G. Acosta, F. A. Nava, I. Méndez, J. Carlos, R. E. García-Arthur, and M. Alvarez (2000). A detailed microseismicity study and current stress regime in the Peninsular Ranges of northern Baja California, Mexico: The Ojos Negros region, *Bull. Seismol. Soc. Am.* **90,** no. 5, 1133–1142.

Glowacka, E., O. Sarychikhina, F. Suárez, F. Alejandro Nava, and R. Mellors (2009). Anthropogenic subsidence in the Mexicali Valley, Baja California, Mexico, and slip on the Saltillo fault, *Environ. Earth Sci.* **59,** no. 7, 1515–1524.

Gonzalez-Garcia, J. J., J. A. Gonzalez Ortega, Y. Bock, Y. Fialko, E. J. Fielding, J. Fletcher, J. E. Galetzka, K. W. Hudnut, L. Munguia, S. M. Nelson, *et al.* (2010). Seismotectonics of the 2010 El Mayor Cucapah—Indiviso earthquake and its relation to seismic hazard in southern California, presented at the *2010 Fall Meeting, AGU*, San Francisco, California, Abstract T53B-2117, available at http://abstractsearch.agu.org/meetings/2010/FM/T53B.html (last accessed June 2017).

Gonzalez-Garcia, J. J., L. Prawirodirdjo, Y. Bock, and D. Agnew (2003). Guadalupe Island, Mexico as a new constraint for Pacific plate motion, *Geophys. Res. Lett.* **30,** no. 16, 1872.

Gonzalez-Ortega, A., Y. Fialko, D. Sandwell, F. Alejandro Nava-Pichardo, J. Fletcher, J. Gonzalez-Garcia, B. Lipovsky, M. Floyd, and G. Funning (2014). El Mayor-Cucapah (M_w 7.2) earthquake: Early

near-field postseismic deformation from InSAR and GPS observations, *J. Geophys. Res.* **119,** 1482–1497.
Hackl, M., R. Malservisi, and S. Wdowinski (2009). Strain rate patterns from dense GPS networks, *Nat. Hazards Earth Syst. Sci.* **9,** 1177–1187.
Haines, A. J., and W. E. Holt (1993). A procedure for obtaining the complete horizontal motions within zones of distributed deformation from the inversion of strain-rate data, *J. Geophys. Res.* **98,** no. B7, 12,057–12,082.
Hauksson, E., J. Stock, L. K. Hutton, W. Yang, J. A. Vidal-Villegas, and H. Kanamori (2010). The 2010 M_w 7.2 El Mayor–Cucapah earthquake sequence, Baja California, Mexico and southernmost California, USA: Active seismotectonics along the Mexican Pacific margin, *Pure Appl. Geophys.* **168,** nos. 8/9, 1255–1277.
Herring, T. (2003). Matlab tools for viewing GPS velocities and time series, *GPS Solut.* **7,** no. 3, 194–199.
Herring, T. A., R. W. King, M. A. Floyd, and S. C. McClusky (2015). *Introduction to GAMIT/GLOBK*, Release 10.6, Mass. Inst. of Technol., Cambridge, Massachusetts.
Huang, M. H., E. J. Fielding, H. Dickinson, J. Sun, J. A. Gonzalez-Ortega, A. M. Freed, and R. Burgmann (2016). Fault geometry inversion and slip distribution of the 2010 M_w 7.2 El Mayor–Cucapah earthquake from geodetic data, *J. Geophys. Res.* **122,** 607–621.
Hutton, K., J. Woessner, and E. Hauksson (2010). Earthquake monitoring in southern California for seventy-seven years (1932–2008), *Bull. Seismol. Soc. Am.* **100,** no. 2, 423–446.
Kostrov, B. V. (1974). Seismic moment and energy of earthquakes, and seismic flow of rock, *Earth Phys.* **1,** 23–40.
Kreemer, C., G. Blewitt, and E. C. Klein (2014). A geodetic plate motion and Global Strain Rate Model, *Geochem. Geophys. Geosys.* **15,** no. 10, 3849–3889.
Lindsey, E., and Y. Fialko (2016). Geodetic constraints on frictional properties and earthquake hazard in Imperial Valley, southern California, *J. Geophys. Res.* **121,** 1097–1113.
Lyons, S. N., Y. Bock, and D. T. Sandwell (2002). Creep along the Imperial fault, southern California, from GPS measurements, *J. Geophys. Res.* **107,** no. B10, 2249–2261.
Masson, F., J. Chery, D. Hatzfeld, J. Martinod, P. Vernant, F. Tavakoli, and M. Ghafory-Ashtiani (2005). Seismic versus aseismic deformation in Iran inferred from earthquakes and geodetic data, *Geophys. J. Int.* **160,** no. 1, 217–226.
Mazzotti, S., L. J. Leonard, J. F. Cassidy, G. C. Rogers, and S. Halchuck (2011). Seismic hazard in western Canada from GPS strain rate versus earthquake catalog, *J. Geophys. Res.* **116,** no. B12310, doi: 10.1029/2011JB008213.
Meade, B. J., and B. Hager (2005). Spatial localization of moment deficits in southern California, *J. Geophys. Res.* **110,** no. B4, doi: 10.1029/2004JB003331.
Molnar, P. (1979). Earthquake recurrence intervals and plate tectonics, *Bull. Seismol. Soc. Am.* **69,** 115–133.
Pancha, A., J. G. Anderson, and C. Kremmer (2006). Comparison of seismic and geodetic scalar moment rates across the Basin and Range Province, *Bull. Seismol. Soc. Am.* **96,** no. 1, 11–32.
Platnner, C., R. Malservisi, T. H. Dixon, P. LaFemina, G. F. Sella, J. Fletcher, and F. Suarez-Vidal (2007). New constrains on relative motion between the Pacific Plate and Baja California microplate (Mexico) from GPS measurements, *Geophys. J. Int.* **170,** no. 3, 1373–1380.
Pollitz, F., R. Burgmann, and W. Thatcher (2012). Illumination of the rheological mantle heterogeneity by the M 7.2 El Mayor–Cucapah earthquake, *Geochem. Geophys. Geosys.* **13,** no. Q06002, doi: 10.1029/2012GC004139.
Rockwell, K. T., J. Fletcher Mackrain, O. Teran, A. P. Hernández Flores, K. Mueller, J. B. Salisbury, S. Akciz, and P. Stepancikova (2015). Reassessment of the 1892 Laguna Salada earthquake: Fault kinematics and rupture patterns, *Bull. Seismol. Soc. Am.* **105,** no. 6, 2885–2893.
Sabadini, R. (2009). Plate deformation, in *Crust and Lithosphere Dynamics: Treatise on Geophysics*, A. B. Watts and G. Shubert (Editors), Vol. 6, Elsevier, Amsterdam, The Netherlands, 153–215.
Samsonov, S. V., W. Feng, and Y. Fialko (2017). Subsidence at Cerro Prieto Geothermal Field and postseismic slip along the Indiviso fault from 2011 to 2016 RADARSAT-2 DInSAR time series analysis, *Geophys. Res. Lett.* **44,** 2716–2724.
Sandwell, D., and P. Wessel (2016). Interpolation of 2-D vector data using constraints from elasticity, *Geophys. Res. Lett.* **43,** 10,703–10,709.
Sarychikhina, O., E. Glowacka, R. Mellors, and F. Suárez Vidal (2011). Land subsidence in the Cerro Prieto Geothermal Field, Baja California, Mexico, from 1994 to 2005: An integrated analysis of DInSAR, leveling and geological data, *J. Volcanol. Geoth. Res.* **204,** nos. 1/4, 76–90.
Savage, J. C., and R. W. Simpson (1997). Surface strain accumulation and the seismic moment tensor, *Bull. Seismol. Soc. Am.* **87,** 1345–1353.
Savage, J. C., M. Lisowski, N. E. King, and W. K. Gross (1994). Strain accumulation along the Laguna Salada fault, Baja California, Mexico, *J. Geophys. Res.* **99,** no. B9, 18,109–18,116.
Shen, Z.-K., R. W. King, D. C. Agnew, M. Wang, T. A. Herring, D. Dong, and P. Fang (2011). A unified analysis of crustal motion in Southern California, 1970–2004: The SCEC crustal motion map, *J. Geophys. Res.* **116,** no. B11402, doi: 10.1029/2011JB008549.
Smith-Konter, B. R., D. T. Sandwell, and P. Shearer (2011). Locking depths estimated from geodesy and seismology along the San Andreas fault system: Implications for seismic moment release, *J. Geophys. Res.* **116,** no. B06401, doi: 10.1029/2010JB008117.
Southern California Earthquake Center (SCEDC) (2013). *Southern California Earthquake Center, Caltech*, Dataset, doi: 10.7909/C3WD3xH1.
Spinler, J. C., R. A. Bennett, C. Walls, S. Lawrance, and J. J. Gonzalez-Garcia (2015). Assessing long-term postseismic deformation following the M_w 7.2 4 April 2010, El Mayor–Cucapah earthquake with implications for lithospheric rheology in the Salton trough, *J. Geophys. Res.* **120,** 3664–3679.
Turcotte, D., and G. Shubert (2002). *Geodynamics*, Cambridge Univ. Press, New York, New York, 456 pp.
Wallace, R. E. (1990). The San Andreas fault system, California, *U.S. Geol. Surv. Profess. Pap. 1515*, 283 pp.
Ward, S. N. (1998). On the consistency of earthquake moment rates, geological fault data, and space geodetic strain: The United States, *Geophys. J. Int.* **134,** no. 1, 172–186.
Wdowinski, S., Y. Sudman, and Y. Bock (2001). Geodetic detection of active faults in S. California, *Geophys. Res. Lett.* **28,** no. 12, 2321–2324.
Wessel, P., and D. Bercovici (1998). Interpolation with splines in tension: A Green's function approach, *Math. Geosci.* **30,** no. 1, 77–93.
Wessel, P., W. H. F. Smith, R. Scharroo, J. Luis, and F. Wobbe (2013). Generic mapping tools: Improved version released, *Eos Trans. AGU* **94,** no. 45, 409–410.
Xu, X., D. T. Sandwell, E. Tymofyeyeva, A. Gonzalez-Ortega, and X. Tong (2017). Tectonic and anthropogenic deformation at the Cerro Prieto Geothermal step-over revealed by Sentinel-1A InSAR, *IEEE Trans. Geosci. Remote Sens.* **55,** no. 1, 9.

J. Alejandro González-Ortega
J. Javier González-García
División de Ciencias de la Tierra
Centro de Investigación Científica y de Educación Superior de Ensenada
22860 Ensenada, Baja California
Mexico
aglez@cicese.mx

David T. Sandwell
Scripps Institution of Oceanography
UC San Diego
La Jolla, California 92093-0225 U.S.A.

Published Online 14 February 2018